FOURTEENTH EUROPEAN ROTORCRAFT FORUM

Paper No. 2

CFD AND TRANSONIC HELICOPTER SOUND

T. W. PURCELL

U.S. ARMY AEROFLIGHTDYNAMICS DIRECTORATE, AVSCOM
AMES RESEARCH CENTER, MOFFETT FIELD, CALIFORNIA, USA

20-23 September, 1988
MILANO, ITALY

CFD AND TRANSONIC HELICOPTER SOUND

Timothy W. Purcell

U.S. Army Aeroflightdynamics Directorate, AVSCOM
Ames Research Center, Moffett Field, California, USA

ABSTRACT

A computational method which predicts far-field impulsive noise from a transonic rotor blade is demonstrated. This method couples near-field results from a full-potential finite-difference method with a new Kirchhoff integral formulation to extend the finite-difference results into the acoustic far-field. This Kirchhoff formula is written in a blade-fixed coordinate system. It requires initial data from the potential code on a plane at the sonic radius. A recent hovering rotor experiment is described where accurate pressure measurements were recorded on the sonic cylinder and at 2 and 3 radii. The potential code prediction of sonic cylinder pressures is excellent. Acoustic far-field pressure predictions show good agreement with hover experimental data over the range of speeds from 0.85 to 0.92 tip Mach number. The latter of which have delocalized transonic flow. These results are some of the first successful predictions for peak pressure amplitudes using a computational code.

1. INTRODUCTION

There are two major sources of high-intensity noise associated with helicopter rotors, Blade-Vortex Interaction noise (BVI), and High-Speed Impulsive noise (HSI). This paper examines a prediction method for the latter type of noise. During HSI noise in high-speed forward flight, the advancing rotor tip creates a shock that radiates forward of the helicopter, or delocalizes. Fortunately, this forward flight problem is well simulated in hover when the tip Mach number nears the forward flight advancing tip Mach number. This delocalization occurs when the supersonic flow region at the blade tip connects to the far field beyond the sonic cylinder. The sonic cylinder is defined by the radius beyond which the undisturbed flow appears to be supersonic to an observer on the blade. This radius is given by R/M, that is the blade radius divided by tip Mach number. Fig. 1 shows the sudden change in the 3 radii pressure as the flow delocalizes from the rotor tip.[1] At delocalization, the pocket of supersonic flow at the blade tip suddenly extends from the blade to connect to the sonic cylinder. This connects the blade to the supersonic far field, which is actually not moving, but, due to a blade-fixed transformation, it appears to be moving supersonically relative to the blade. This mathematical transformation also changes the equations to a hyperbolic form meaning waves are carried along characteristic lines.

Linear methods have consistently underpredicted the far-field acoustic levels for high tip Mach numbers. The theory developed by Ffowcs Williams and Hawkings[2] improves upon linear formulations by including the nonlinear quadrupole term in the acoustic pressure. Several methods have been developed for evaluating this quadrupole term[3-5], but they are hampered by difficulties concerning interpretation of this quadrupole term, physical modeling of this term, convergence problems of the integral, and integration volume determination. To

date, neither computer codes nor integral techniques have been able to successfully predict the far-field acoustic pressures associated with high-speed, delocalized rotor flows using the Ffowcs Williams - Hawkings equation.

Many computational fluid dynamics (CFD) codes exist which solve the non-linear flow-field found on high-speed rotors.[6-10] Typically these codes are well developed for surface pressure and flow-field predictions close to the blade. Far from the blade however, the grid resolutions are insufficient to resolve the details of the acoustic pressure field. Extending these codes for acoustic prediction is very costly due to the huge grids required and instability problems may result from increasing the size of the computational domain. For artificial density methods used with a potential code, these instabilities increase with radial distance from the rotor blade just as the relative Mach number increases.[11] However, potential codes are well developed for rotor blade applications and are currently very efficient.

This paper combines a modification of an efficient potential code with a new non-linear Kirchhoff formulation for prediction of the acoustic far field. The potential code is FPR, which stands for Full-Potential Rotor code. It solves the fully conservative, three-dimensional, unsteady form of the full-potential equation and is described in Refs. 8 and 9. The FPR code predicts the flow quantities on the blade and on a plane located at the sonic radius. The new Kirchhoff integral known as Isom's equation is developed by Isom et al. in reference 12. This non-linear formula uses surface integrals of the pressure and velocity results at the sonic cylinder to determine the acoustic pressures in the far field. It treats the linear sonic cylinder as the sole source of all acoustics information. This data is then propagated to the far field assuming a constant speed of sound.

The main objective of this paper is to look at this combined CFD/integral equation approach in more detail than has been done in the past. A number of questions will be answered. First, how good is the FPR prediction at the sonic cylinder? An experiment was performed to provide sonic cylinder data for evaluating the accuracy of FPR. Secondly, how does this experiment compare with a similar experiment cited in reference 13 that had no sonic cylinder data recorded? Lastly, how good is the far-field prediction of acoustic pressure?

2. THE FULL-POTENTIAL ROTOR CODE

The Full-Potential Rotor code (FPR) solves the unsteady full-potential equation in strong conservation form. This equation is written below in generalized coordinates.

$$\frac{\partial}{\partial \tau}\left(\frac{\rho}{J}\right) + \frac{\partial}{\partial \xi}\left(\frac{\rho U}{J}\right) + \frac{\partial}{\partial \eta}\left(\frac{\rho V}{J}\right) + \frac{\partial}{\partial \zeta}\left(\frac{\rho W}{J}\right) = 0 \qquad (1)$$

with density given by:

$$\rho = \left\{ 1 + \frac{\gamma - 1}{2}\left[-2\Phi_\tau - (U + \xi_t)\Phi_\xi - (V + \eta_t)\Phi_\eta - (W + \zeta_t)\Phi_\zeta\right] \right\}^{1/\gamma - 1} \qquad (2)$$

U, V and W are the conventional contravariant velocities for the body fitted grid. All velocities are normalized by a_0, the free-stream acoustic velocity, distances

2-3

by the airfoil chord length, c, and time by the combination (c/a_∞). Density is normalized by the free-stream value. Further details of these equations and the associated metrics, A_n, and contravariant velocities are described by Strawn and Caradonna in Ref. 8.

Equation (1) is solved using first-order backward differencing in time and second-order central differencing in space. The temporal density derivative is locally linearized about the old time levels in a manner that preserves the conservative form. The resulting equation is approximately factored into ξ, η, and ζ operators. The steady-state version of this equation can be written as

$$\left[I + hU^n \delta_\xi \pm Dh\bar{\delta}_\xi - \frac{h^2}{\hat{\beta}^n} \delta_\xi (\hat{\rho}A_1)^n \delta_\xi \right] \times \left[I + hV^n \delta_\eta - \frac{h^2}{\hat{\beta}^n} \delta_\eta (\hat{\rho}A_2)^n \delta_\eta \right] \times$$

$$\left[I + hW^n \delta_\zeta \pm Eh\bar{\delta}_\zeta - \frac{h^2}{\hat{\beta}^n} \delta_\zeta (\hat{\rho}A_3)^n \delta_\zeta \right] \Delta\Phi^n = \tag{3}$$

$$\frac{h^2}{\hat{\beta}^n} \left[\delta_\xi (\hat{\rho}U)^n + \delta_\eta (\hat{\rho}V)^n + \delta_\zeta (\hat{\rho}W)^n \right]$$

where δ_ξ, δ_η, and δ_ζ represent central-difference operators in space. $\Delta\Phi^n$ is the correction term used to update the potential, Φ, to its final steady-state value. A steady state ADI relaxation algorithm solves this factored equation.

A new version of the FPR code is used in the calculations here. The differences between version one and two of FPR include: (1.) Half-point differencing formulas are used for both density and metric calculations. This improvement over the nodal differencing used in version 1 increases the robustness and accuracy of the code. (2.) A monotonic density biasing scheme which improves the high-speed behavior of the code has been added. Some details of this new version are covered by Caradonna et al. in reference 15.

A sample grid for a rotor calculation appears in Fig. 2. An O-grid has been chosen for the basic finite-difference grid because of its efficient use of grid points. Rotor flows are computed by assigning an appropriate rotational coordinate velocity to each grid point. These coordinate velocities are given by ξ_t, η_t, and ζ_t. As a result, the rotor and the attached finite-difference grid move through still air and the velocity potential, Φ, is equal to zero in the far field and acts as a non-rotating perturbation to the rotating flow. Fig. 3 shows the top view of a grid typical of the large region needed for acoustic predictions. In this case, the outer boundary is placed very far away to absolutely avoid contamination of the solution at the sonic cylinder. Fig. 2 also shows the boundary conditions that are used. At the outer radial boundary of the O-grid, a nonreflection condition prevents the accumulation of disturbances. This boundary condition is described in Ref. 9. On the surface of the blade, a transpiration condition simulates any angle of attack conditions. Along the inner boundary plane, normal to the rotor, the span-wise contravariant velocity, V, is set equal to η_t. Since this study only uses non-lifting conditions, no other details of lifting boundary conditions and circulation convection are reviewed here.

The stream-wise flux terms use upwind density biasing in regions of supercritical flow to ensure stability of the algorithm. The density is biased in both ζ and the ξ directions and it is biased upwind no matter how the grid lines are

oriented to the freestream. However, instabilities are still possible. As the finite-difference grid extends radially beyond the sonic cylinder, the free-stream flow relative to the blade becomes supersonic and the full-potential equation becomes hyperbolic. The FPR code uses central-differencing in space with an upwind-biased artificial density in regions of supersonic flow. This method has been shown in Ref. 11 to give stability problems in regions where the free-stream flow is supersonic. A set of damping terms has been added to FPR for extra stability in highly supersonic regions. The parameters D and E control how much damping is added in the ξ and ζ directions respectively. The $\bar{\delta}$ is a finite-difference operator chosen so that it always adds upwind data to the system. The effect of these coefficients is to increase the diagonal dominance in the solution matrices. These damping terms approach zero as the solution converges to a steady-state result, but, this modification to the FPR code ensures a stable convergence at outer radial stations for cases where the local Mach number is well above one.

3. THE ISOM EQUATION

The Kirchhoff equation called the Isom equation uses non-rotating surface integrals of pressure and velocity. This approach has several practical advantages over previous methods. A large volume of quadrupole integral is replaced by a surface integral over the sonic cylinder surface. This control surface is a non-rotating one, eliminating mathematical singularities of the Ffowcs Williams and Hawkings equation, although, another singularity arises which is discussed later. More importantly, the close proximity of the sonic cylinder to the rotor tip means that the finite-difference code only needs to solve the near-field region around the tip.

The geometrical acoustics approximation can be based on the small-disturbance potential equation. One form of this equation is

$$\frac{\phi_{t't'}}{a_0^2} - \nabla^2 \phi = -\frac{\partial Q}{\partial t'} \tag{4}$$

The time-differentiated second order nonlinearity Q is given by

$$Q = \left(\frac{\gamma - 1}{2a_0^4}\right)\phi_{t'}^2 + \frac{1}{a_0^2}|\nabla\phi|^2 \tag{5}$$

where γ is the ratio of specific heats and a_0 is the sound speed in undisturbed air. Note that Eqns. (4) and (5) assume that the local sound speed is constant.

The objective is to use Eqn. (4) to find the far-field disturbance pressure in terms of nonlinear initial data on some surface near the blade tip. This is accomplished by using a Kirchhoff solution to Eqn. (4) that converts it to an integral equation with Q as a source term. Next, a stationary phase approximation is applied that reduces the domain of all integrals to that of a data surface near the tip. This initial data is determined from the finite-difference code that solves the full-potential equation in the region close to the blade tip. The advantage of the geometrical acoustics approximation is that the finite-difference computation need not be continued from the blade surface all the way into the acoustic field.

Details of the solution of Eqn. (4) are quite lengthy and its derivation is shown by Isom in Ref. 12.

Fig. 4 shows the important coordinate directions used in the following equations. Of particular note is the β coordinate which measures the distance to the observer along a line tangent to the sonic cylinder. Whenever β is used it is in units of radii measured along a line tangent to the sonic cylinder between the observer and the sonic cylinder. All other observer distances are the usual measure of distance to the rotor hub.

Eqn. (4) can be solved for the acoustic pressure at a point in the far field. The resulting formula for acoustic pressure is given below.

$$
\begin{aligned}
p(\beta, T) = &\rho_0 a_0^2 \frac{6^{2/3} M \epsilon}{36 \pi \beta} \iint_S \frac{P(T', Z_0) - P(\sigma, Z_0)}{T' - \sigma} \frac{sgn(T' - \sigma)}{|T' - \sigma|^{1/3}} \, d\sigma \, dZ_0 \\
&- \rho_0 a_0^2 \frac{M \epsilon}{6^{2/3} 3 \pi \beta} \iint_S \frac{G(T', Z_0) - G(\sigma, Z_0)}{T' - \sigma} \frac{1}{|T' - \sigma|^{2/3}} \, d\sigma \, dZ_0
\end{aligned}
$$

(6)

$$
G(T, Z_0) \equiv M \, V_r(T, Z_0) + \frac{\gamma + 1}{2 \dot{g}} P^2(T, Z_0)
$$

where $p(\beta, T)$ is the far-field disturbance pressure. ρ_0 and a_0 are the freestream density and acoustic velocity, respectively. γ is the ratio of specific heats. M is the tip Mach number. ϵ is the inverse of the aspect ratio R, also defined as span/chord. β is the distance to an observer along a line tangent to the sonic cylinder and is defined by $\beta = [(\omega r / a_0)^2 - 1]^{1/2}$ where $\omega =$ blade angular speed, and $r =$ dimensional distance along the rotor in the span-wise direction. T and σ are azimuthal distances. T is a characteristic variable defined as $T = (1/\epsilon)(\theta + \beta - \tan^{-1} \beta)$ where θ is the angle relative to the blade along the sonic cylinder in radians. Z_0 is a scaled vertical distance $= z \epsilon^{-2/3} \omega / a_0$. $V_r = \Phi_y$, $P = (\rho_0 a_0^2 \epsilon^{2/3})^{-1} p$, and $\Phi = (a_0 c \epsilon^{2/3})^{-1} \phi$. The value $\dot{g}$ is the slope of any shock that may cross the linear sonic cylinder. For lower Mach number cases, there is no shock at the sonic cylinder and this P^2 term is dropped due to the very small contributions from this nonlinear term. The location for the pressure evaluation is determined by the values of β and T and the results of this equation are limited to the plane of rotation although Isom has expanded it to off the rotor plane.[12] Finally, the surface integrals, S, in Eqn. (6) are located at the sonic cylinder ($r = a_0 / \omega$). Choosing this location for initial data greatly simplifies the result.

The FPR solution produces pressure data at the sonic cylinder on an O-grid plane of data perpendicular to the rotor axis. This solution is then interpolated onto a rectangular mesh for ease of integration. Since this plane does not lie on a constant radial station, a small approximation is introduced here which greatly simplifies the integration. The simplification has negligible effect since most of the important data lies on a region of the sonic cylinder that is almost parallel to the plane of data from FPR. The integrals then use the rectangular mesh data for input. A bi-cubic spline smoothly interpolates the data between points on the mesh. A domain of ±3.5 chords in both the vertical and horizontal directions provides sufficient data for the integration.

The integrals in Eqn. (6) contain singularities when $T = \sigma$ which can create problems. The equations are integrated in the σ direction up to a small

distance from the singularity. The contributions at the singularity are computed separately. The first integrand can be shown to be symmetric and odd at the singularity. Hence, its integrated contribution is zero. The first integrand is even, with a non-canceling contribution near the singularity. This region near the singularity responds favorably to an integration by parts method after removing the basic derivative looking term from the integral.

4. AN EXPERIMENT IN NEAR FIELD ROTOR ACOUSTICS

Fig. 5 shows a top view of the configuration used in this experiment. The rotor used in this hover test is a $1/7^{th}$ scale model of a UH-1H main rotor with straight untwisted blades and a NACA 0012 airfoil section. This rotor is 41.14 inches in radius with a 3 inch chord. These same blades were used some 10 years ago as described by Boxwell in Ref. 13. This model was run at high-speed hover with thrust set to a low level in order to minimize the wake influence. Acoustic pressure data was measured in the plane of the rotor at radial locations of: R/M (the sonic cylinder), $2.18R$, and $3.09R$ for tip Mach numbers of $M = 0.85$, $M = 0.88$, $M = 0.90$, $M = 0.92$, and $M = 0.95$. The sonic cylinder microphone (mic) was mounted on a traverse mechanism to allow precise positioning of this mic location with changes in Mach number.

Careful monitoring of the room temperature and humidity allow exact specification of the needed rotor speed for a specific Mach number. The rotor RPM was stabilized to ± 1 RPM out of a typical rotor speed of 2900 RPM. A cyclic control unit allowed exact positioning of the rotor tip path relative to the mic array. This positioning was checked by mounting a foam block to the traverse which was SLOWLY moved toward the rotor tip circle after the rotor was brought to operating speed. The notch cut in the brittle foam validated the position of the rotor tip.

The mics in this test were B&K (Brüel & Kjær) 4136 pressure mics designed for strong impulsive noises. These mics were chosen for their high sound level capability and excellent phase accuracy. Their amplitude accuracy is also very good. All mics were from the same production batch. The mics were calibrated electrostatically with the same preamplifier-cable-power/supply assembly used in the experiment. These calibration results were well within the claimed design specifications of B&K.

No analogue tape recorder was involved in the results shown here. Due to the phase error of most FM (frequency modulation) tape recorders, a direct digitization of the mic signals was used. A high-accuracy digitizing unit with 32K parts of resolution was used with phase accurate conditioning filters.

The next several figures compare the results from this test, the 1988 AHC (Anechoic Hover Chamber) test, and the 1978 AHC test described by Boxwell.[13] As stated before the 1988 AHC results are actually at $3.09R$ so a correction factor has been used in all of the following 1988 $3R$ results. For the $3.09R$ measurements for Mach numbers less than 0.92, the amplitudes have been increased 3.5%. For Mach numbers of 0.92 and above, the amplitudes have been increased 3.4%. These factors are found by a $1/\beta$ type correction factor using the β distance described earlier in the acoustics equations section. A similar correction was applied to the $2.18R$ data to correlate it with the usual $2R$ data measurements.

Fig. 6 shows a comparison of the 1988 AHC test with some of the data points from the 3R location of the 1978 AHC test. Fig. 6a shows the $M = 0.85$ results from just the 1988 test. Almost all of the test data agree well as shown in Fig. 6b for the $M = 0.88$ case. The $M = 0.85$ pressure peaks were all a little low as shown later. The agreement at $M = 0.90$ is almost exact as shown in Fig. 6c. Here the rotor tip flow has just started delocalization and is very sensitive to rotor speed and room recirculation effects, if any. The next figure, Fig. 6d, compares the results for $M = 0.93$ from the 1978 test with $M = 0.92$ results from the 1988 test. Hence, there is an expected difference in amplitudes. There was no $M = 0.93$ data from the 1988 test. Fig. 6e shows $M = 0.95$ data from the 1988 test where a very strong shock has appeared at the 3R location. At high speed there is less change with Mach number as shown by the smaller jumps between constant Mach lines at the higher Mach numbers in Fig. 7. This figure plots the peak negative amplitudes for various test points as a function of distance β along the line tangent to the respective sonic cylinders at each Mach number. The sonic cylinder radius and therefore this tangent line change with Mach number. Here, again, excellent correlation for all distances is seen for all speeds except $M = 0.85$. This plot of pressure as a function of β demonstrates how important this reference dimension is in rotor acoustics. This concept of β arose out of the theory developed for the Isom equation and correlates quite well with the observed data as seen in Fig. 7. There is an almost straight line relation between pressure peaks and the distance β. Although there are only a few data points shown on this plot, looking at data as a function of β seems to correlate well and shows great promise for rotor acoustics work.

5. COMPUTED PREDICTIONS

Figs. 8a and 8b compare the pressures predicted by FPR at the sonic cylinder with the results obtained from the 1988 hover test. Fig. 8a is typical of the results predicted by FPR. The curve shape is always very similar and in all but the lowest speed cases, the magnitudes are extremely close. This $M = .90$ case shows that FPR predicts a shock on the sonic cylinder. The older version of FPR did not predict a shock, only a slightly non-symmetric waveform. This indicates the higher accuracy from the modifications in this version 2 of FPR. Fig. 8b shows the over-all prediction of sonic cylinder pressure peaks compared with experiment for several Mach numbers. The $M = .85$ case shows a slight underprediction for the FPR peak pressure. This arises from dissipation as this weak signal is computed from the rotor tip to the sonic cylinder almost two chords away. As the signal strength increases, as in the $M = .90$ results, the FPR prediction is much better. The $M = .90$ and higher speed cases show a definite shock on the sonic cylinder and again the correlation in peak amplitudes is excellent. The prediction at $M = .92$ is a little high as the speeds in front of the shock on the blade approach $M = 1.3$ and higher. At these higher speeds, the isentropic assumption used in the potential code breaks down and higher peaks before the shock are expected. Higher speed cases are not developed yet due to interaction problems between the radiating shock and a grid singularity off the blade. The O-grid used in FPR collapses to a zero thickness slit off the blade tip. As the grid wraps around the edge of this slit, certain approximations are necessary since some of the grid metrics are singular there. These approximations create problems for strong flow gradients. These problems of the region off the tip do not affect the solution on

the body however. A new type of grid is under development for this region off the blade tip.

Fig. 8c shows a series of the computed results using Isom's equation with FPR initial data for the $3R$ location. The $M = .88$ case shows an underprediction in peak pressure. The $M = .90$ results agree a little better in peak pressure results. Since this is a linear far-field method, all the predictions at $3R$ directly reflect the input from FPR at the sonic cylinder. Hence, the jump character of the pressure seen at the sonic cylinder is mirrored by the $3R$ pressure. Just before the shock, there is an inflection in the pressure curve. This is unexplained as it is seen in all forms of integration for the far-field pressures. The experimental results clearly do not show this type of ramp before the shock.

The $M = .92$ case clearly shows a shock at all locations. Here the peak level prediction is good. One problem with the current method arises from finding the shock angle at the sonic cylinder for cases with a strong P^2 contribution as in the $M = .90$ and $M = .92$ cases. There is an error of about $\pm 2°$ involved in finding the $\dot{g}$ value of the shock slope, especially in cases such as $M = .90$ where the shock just barely reaches the sonic cylinder. The current method curve fits a first-order curve through the locations of peak minimum densities near the sonic cylinder. This seems to work fairly well but may need improving. The $M = .92$ case has a strong shock at the sonic cylinder which is easy to measure for $\dot{g}$ evaluation. In all cases, predictions are much improved over past methods. Using this method, errors are measured in percentages such as 15, 5, or even 0.7% instead of measuring error by magnitudes using the decibel scale.

Finally, Fig. 9 shows the results obtained from the predictions here and the past predictions using linear and nonlinear quadrupole methods with a range of data taken from hover tests. Parts of this plot are extracted from reference 1. Here the usual deficiency of the linear methods is seen by their underprediction by a factor of two. The quadrupole method does better but still diverges at delocalization near $M = .90$. Only the current method is able to reflect the bend seen in the experimental curve.

6. CONCLUSIONS

A new method has been developed to predict the impulsive noise signature generated by a high-speed transonic rotor blade. The matching of a finite-difference method and a Kirchhoff integral formula combines the advantages of each formulation in the regions where each is most appropriate. A detailed investigation of this combined CFD/integral equation approach has been shown. The FPR prediction at the sonic cylinder has shown excellent agreement with experimental data. The experiment provided the previously unrecorded sonic cylinder data and it correlates well with an earlier experiment when compared with data from the two and three radii locations. The far-field prediction of acoustic pressures correlates well except at the lower speeds where it underpredicts. An important correlation of pressure peaks has been shown by using the distance along a line tangent to the sonic cylinder to the observer.

AKNOWLEDGEMENTS

REFERENCES

1. F. H. Schmitz and Y. H. Yu: "Transonic Rotor Noise—Theoretical and Experimental Comparisons," *Vertica*, Vol. 5, 1982, pp. 55-7.

2. J. E. Ffowcs Williams and D. L. Hawkings: "Sound Generation by Turbulence and Surfaces in Arbitrary Motion," Philos. Trans. R. Roc. London, Ser. A, vol. 264, May 8, 1969, pp. 321-342.

3. M. V. Lowson: "Helicopter Noise: Analysis-Prediction and Methods of Prediction," *AGARD Lecture Series No. 63 on Helicopter Aerodynamics and Dynamics*, 1973.

4. F. H. Schmitz and Y. H. Yu: "Theoretical Modeling of High-speed Helicopter Impulsive Noise," *Journal of the American Helicopter Society*, vol. 24, No. 1, 1979.

5. D. Hawkings: "Noise Generation by Transonic Open Rotors," Westland Helicopters Limited, Research Paper 599, June 1979.

6. I-Chung Chang and C. Tung: "Numerical Solution of the Full-Potential Equation for Rotors and Oblique Wings using a New Wake Model," AIAA Paper 85-0268, January 1985.

7. N. L. Sankar and D. Prichard: "Solution of Transonic Flow Past Rotor Blades Using the Conservative Full-Potential Equation," AIAA Paper 85-5012, October 1985.

8. R. C. Strawn and F. X. Caradonna: "A Conservative Full-Potential Model for Unsteady Transonic Rotor Flows," *AIAA Journal* Vol. 25, No. 2, 1987, pp. 193-198.

9. R. C. Strawn and C. Tung: "Prediction of Unsteady Transonic Rotor Loads with a Full-Potential Rotor Code," *Presented at the 43rd Annual Forum of the American Helicopter Society*, May 1987.

10. T. A. Egolf and S. P. Sparks: "Hovering Rotor Airload Prediction Using a Full-Potential Flow Analysis with Realistic Wake Geometry," *Presented at the 41st Annual Forum of the American Helicopter Society*, May, 1985.

11. T. W. Purcell: "A Computational and Experimental Study of High-Speed Impulsive Noise from a Rotating Cylinder," *Presented at the AIAA Aerospace Sciences Conference*, AIAA paper 87-0253, January 1987, see also Ph.D dissertation, Department of Aeronautics and Astronautics, Stanford University, June 1986.

12. M. P. Isom, T. W. Purcell, and R. C. Strawn: "Geometrical Acoustics and Transonic Helicopter Sound," *Presented at the AIAA 11th Aeroacoustics Conference*, AIAA paper 87-2748, October, 1987.

13. D. A. Boxwell, Y. H. Yu, and F. H. Schmitz: "Hovering Impulsive Noise: Some Measured and Calculated Results," NASA CP-2052, 1978, and *Vertica*, Vol. 3, No. 1, 1979.

14. M. P. Isom: "Acoustic Shock Waves Generated by a Transonic Helicopter Blade," *Presented at the 36th Annual National Forum of the American Helicopter Society*, Paper 63, May 1980.

15. F. X. Caradonna, R. C. Strawn, and J. O. Bridgeman: "An Experimental and Computational Study of Rotor-vortex Interactions," *Presented at the 14th European Rotorcraft Forum*, Paper 18, September 1988.
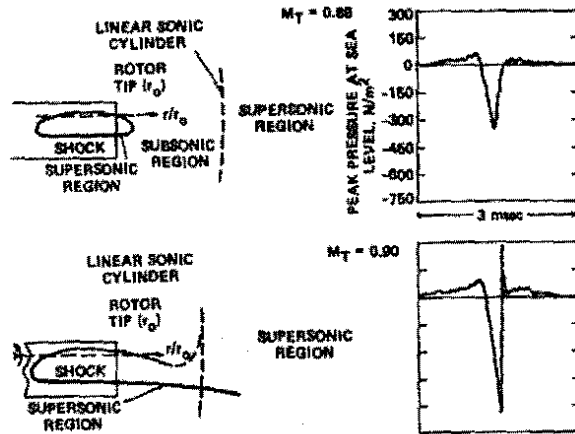
Fig. 1 Delocalization and its effects in the far field.
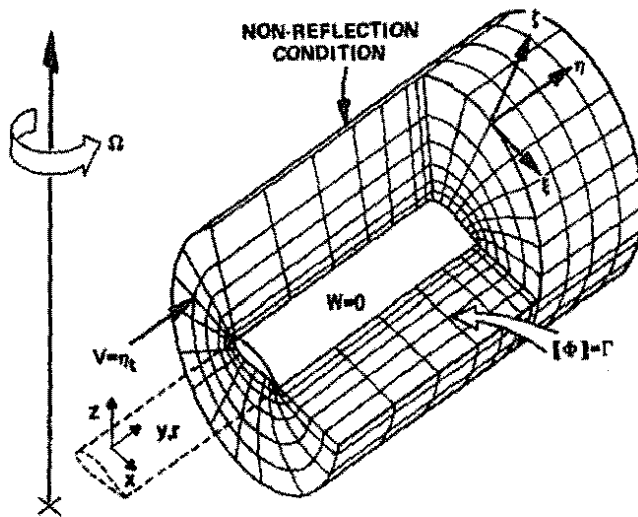
Fig. 2 Grid and boundary conditions for FPR code.
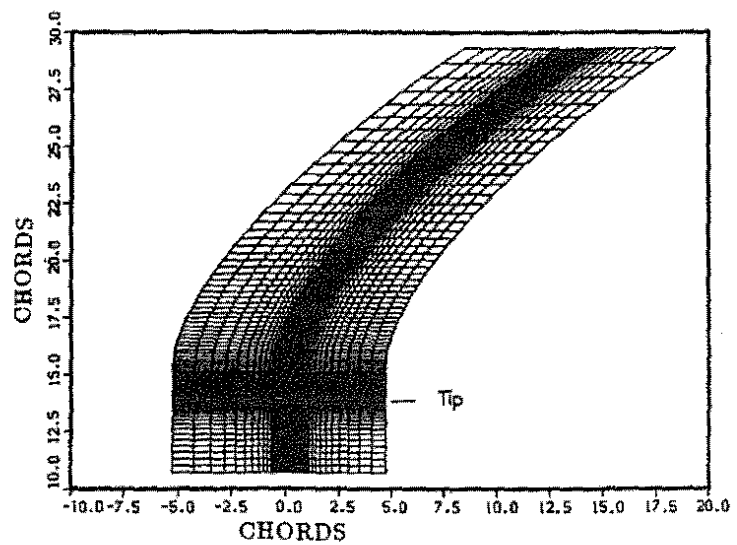
Fig. 3 Top view of grid for acoustics calculations.
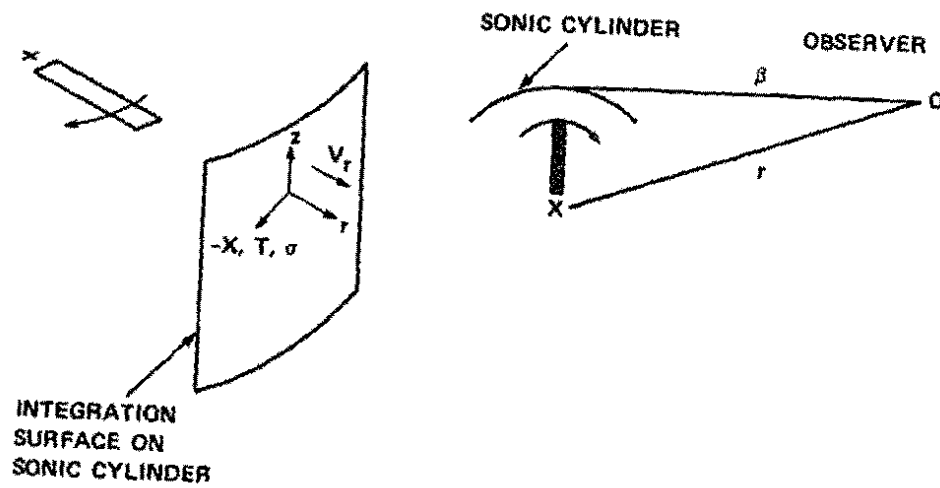
Fig. 4 Coordinate directions used in this paper.
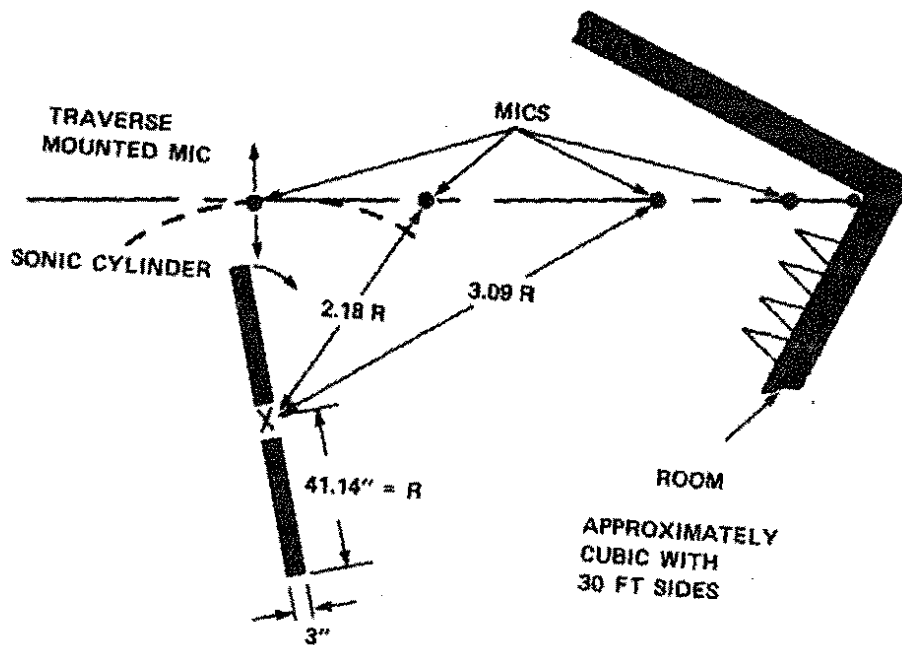
Fig. 5 Top view of the AHC testing room.
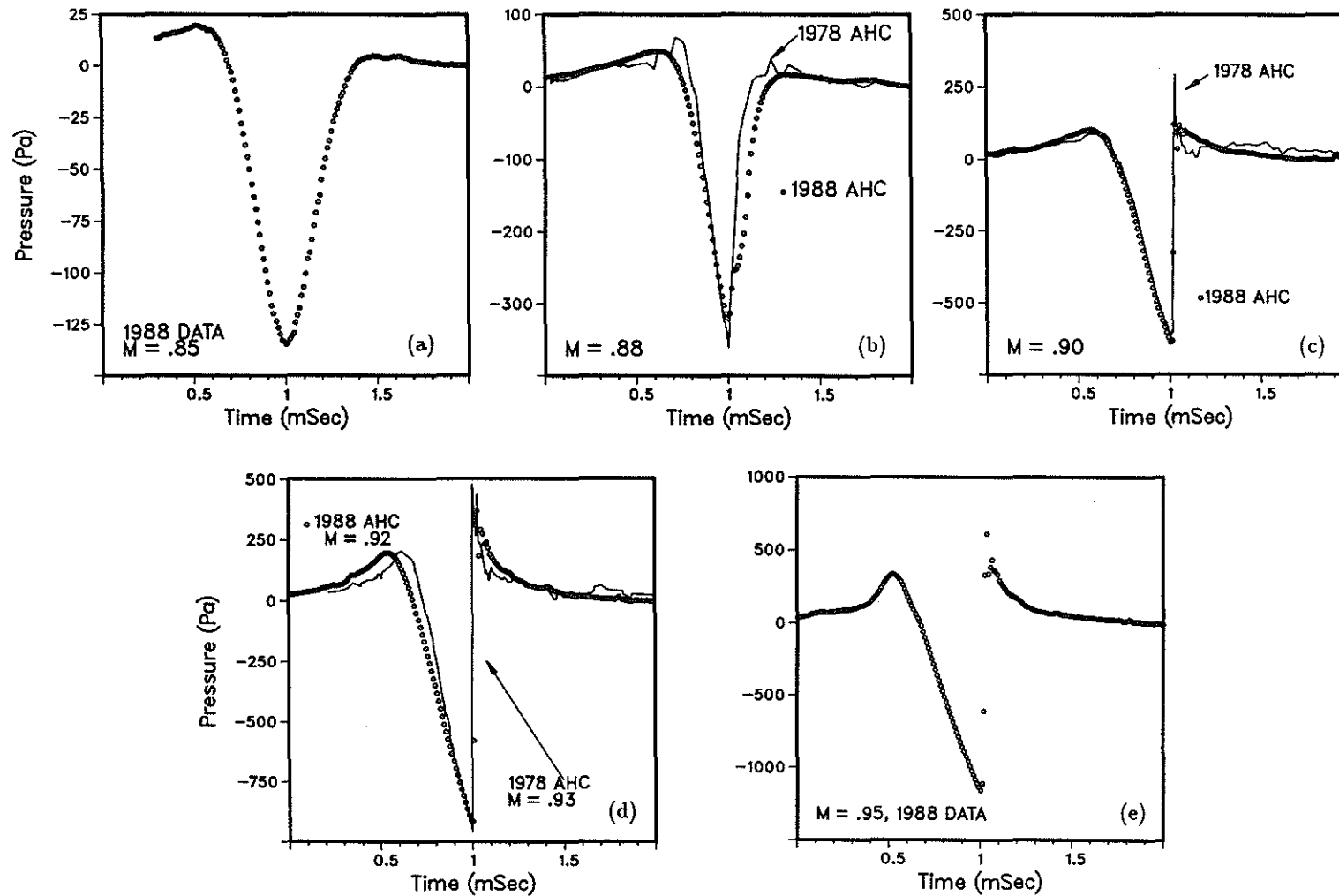
Fig. 6 Pressures at 3R from 1978 and 1988 tests.
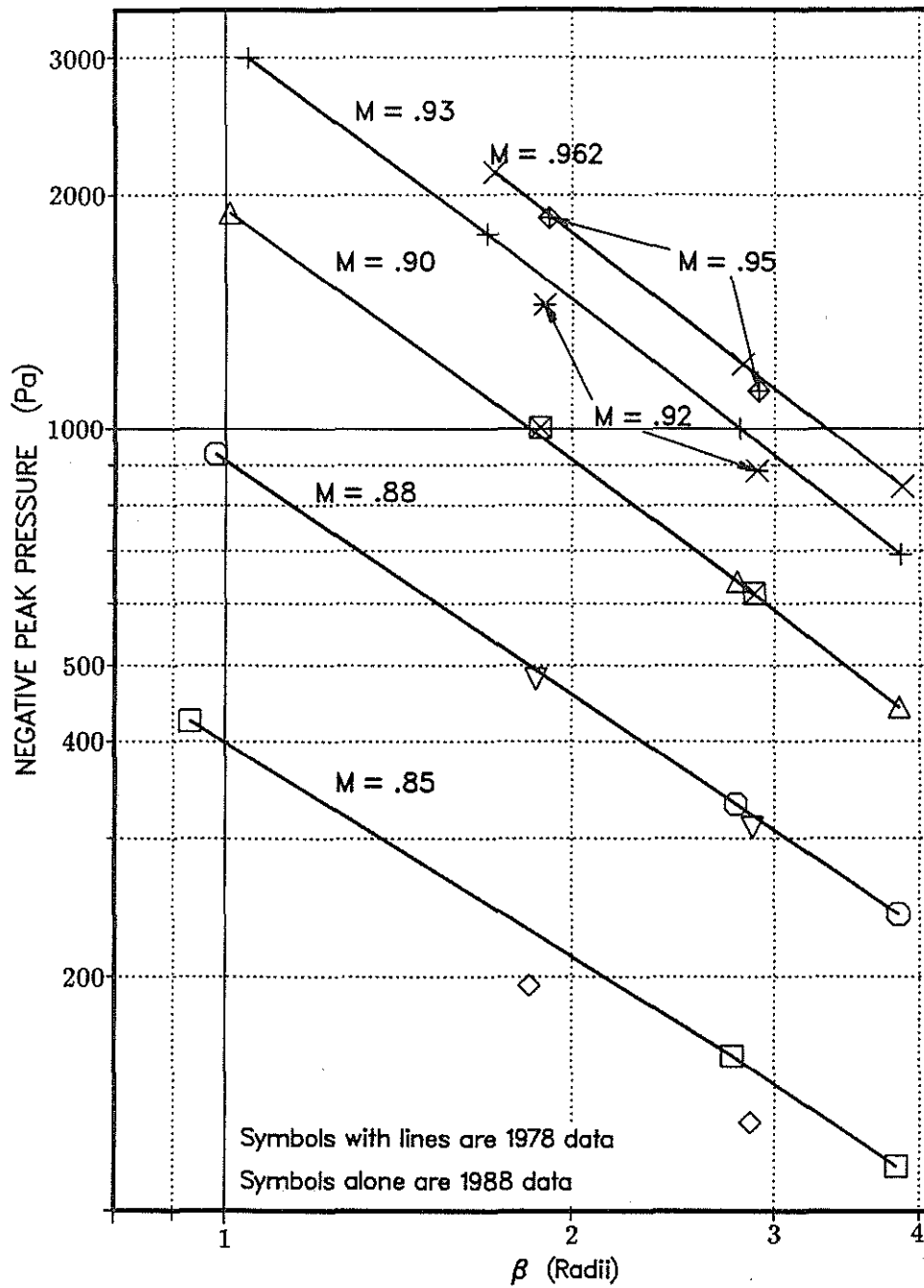
Fig. 7 Pressure peaks from 1978 and 1988 tests.

Sonic Cylinder Data ⟶

8(a)

8(b)

8(c)
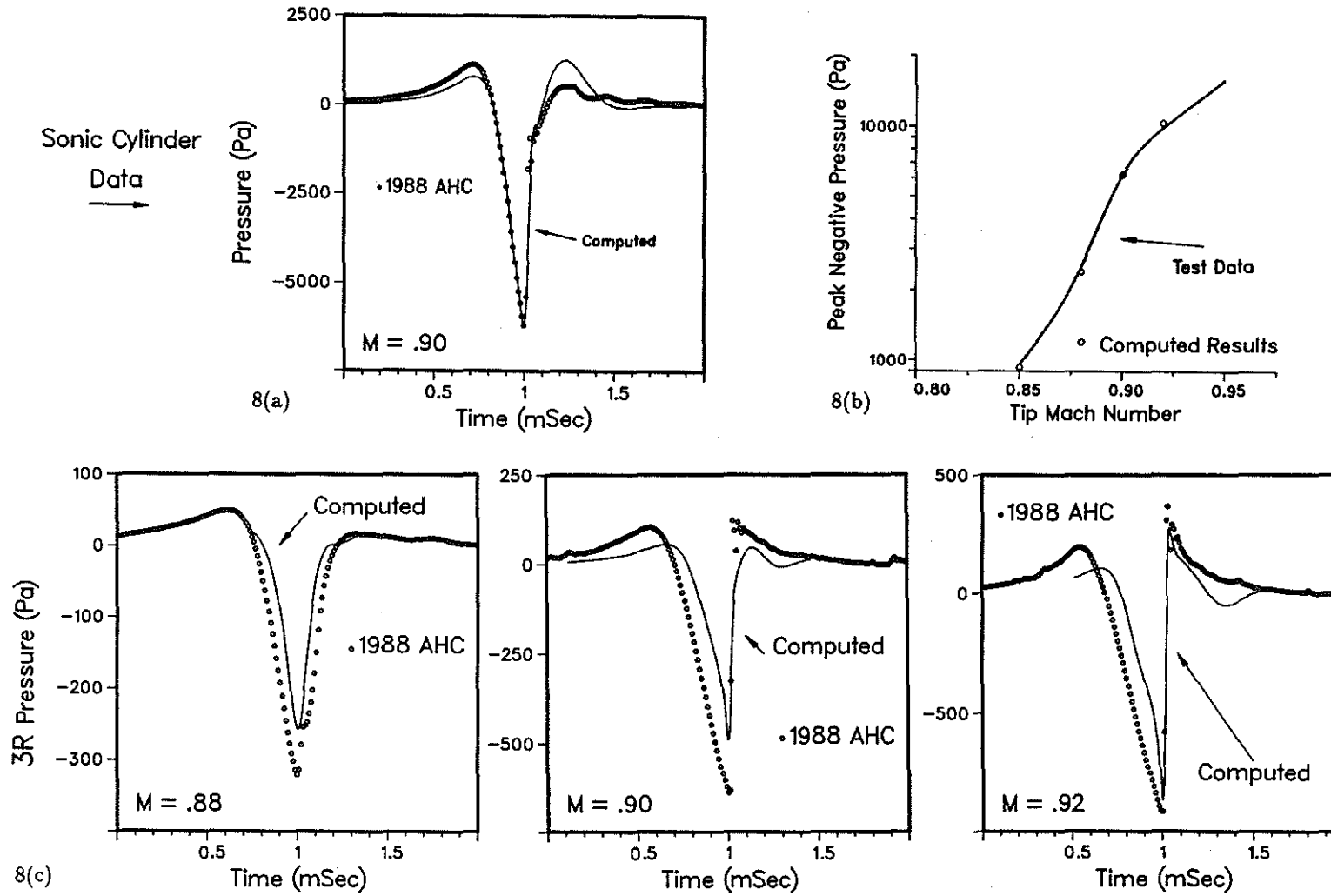
Fig. 8 Pressures from computation and 1988 tests.
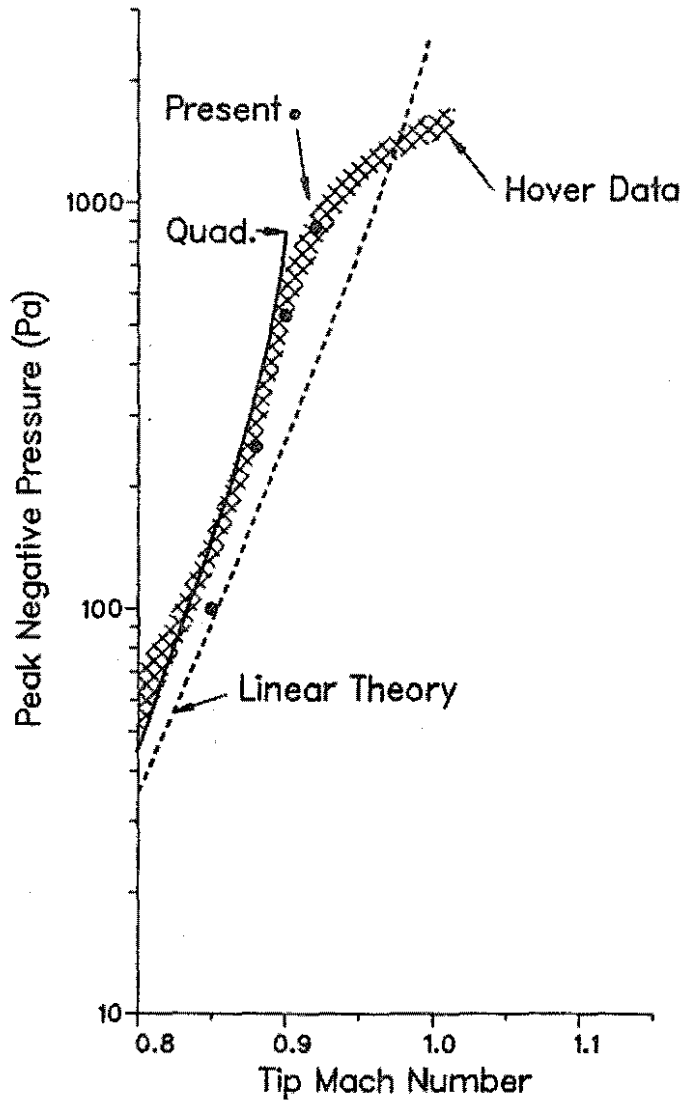
Fig. 9 3R pressure peaks from various sources.